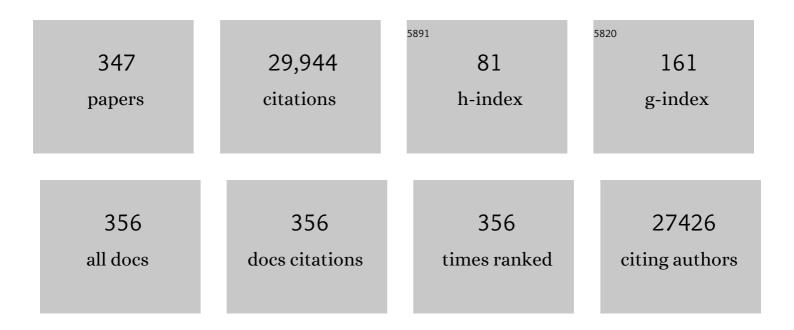
List of Publications by Year in descending order

Source: https://exaly.com/author-pdf/4008967/publications.pdf Version: 2024-02-01



#	Article	IF	CITATIONS
1	Hydrogen evolution by a metal-free electrocatalyst. Nature Communications, 2014, 5, 3783.	5.8	1,851
2	Ti3C2 MXene co-catalyst on metal sulfide photo-absorbers for enhanced visible-light photocatalytic hydrogen production. Nature Communications, 2017, 8, 13907.	5.8	1,496
3	Single Atom (Pd/Pt) Supported on Graphitic Carbon Nitride as an Efficient Photocatalyst for Visible-Light Reduction of Carbon Dioxide. Journal of the American Chemical Society, 2016, 138, 6292-6297.	6.6	985
4	Defect Graphene as a Trifunctional Catalyst for Electrochemical Reactions. Advanced Materials, 2016, 28, 9532-9538.	11.1	961
5	Nanoporous Graphitic-C ₃ N ₄ @Carbon Metal-Free Electrocatalysts for Highly Efficient Oxygen Reduction. Journal of the American Chemical Society, 2011, 133, 20116-20119.	6.6	958
6	A Heterostructure Coupling of Exfoliated Ni–Fe Hydroxide Nanosheet and Defective Graphene as a Bifunctional Electrocatalyst for Overall Water Splitting. Advanced Materials, 2017, 29, 1700017.	11.1	845
7	2D MXenes: A New Family of Promising Catalysts for the Hydrogen Evolution Reaction. ACS Catalysis, 2017, 7, 494-500.	5.5	825
8	Metal-Free Single Atom Catalyst for N ₂ Fixation Driven by Visible Light. Journal of the American Chemical Society, 2018, 140, 14161-14168.	6.6	742
9	Graphene Defects Trap Atomic Ni Species for Hydrogen and Oxygen Evolution Reactions. CheM, 2018, 4, 285-297.	5.8	624
10	Hybrid Graphene and Graphitic Carbon Nitride Nanocomposite: Gap Opening, Electron–Hole Puddle, Interfacial Charge Transfer, and Enhanced Visible Light Response. Journal of the American Chemical Society, 2012, 134, 4393-4397.	6.6	565
11	Understanding the Enhancement in Photoelectrochemical Properties of Photocatalytically Prepared TiO ₂ -Reduced Graphene Oxide Composite. Journal of Physical Chemistry C, 2011, 115, 6004-6009.	1.5	403
12	Organic–inorganic bismuth (III)-based material: A lead-free, air-stable and solution-processable light-absorber beyond organolead perovskites. Nano Research, 2016, 9, 692-702.	5.8	351
13	Graphdiyne: a versatile nanomaterial for electronics and hydrogen purification. Chemical Communications, 2011, 47, 11843.	2.2	329
14	Towards lead-free perovskite photovoltaics and optoelectronics by ab-initio simulations. Scientific Reports, 2017, 7, 14025.	1.6	310
15	Multifunctional Porous Graphene for Nanoelectronics and Hydrogen Storage: New Properties Revealed by First Principle Calculations. Journal of the American Chemical Society, 2010, 132, 2876-2877.	6.6	304
16	A General Twoâ€ S tep Strategy–Based Highâ€Throughput Screening of Single Atom Catalysts for Nitrogen Fixation. Small Methods, 2019, 3, 1800376.	4.6	303
17	Charge Mediated Semiconducting-to-Metallic Phase Transition in Molybdenum Disulfide Monolayer and Hydrogen Evolution Reaction in New 1T′ Phase. Journal of Physical Chemistry C, 2015, 119, 13124-13128.	1.5	295
18	Charge-Controlled Switchable CO ₂ Capture on Boron Nitride Nanomaterials. Journal of the American Chemical Society, 2013, 135, 8246-8253.	6.6	293

#	Article	IF	CITATIONS
19	First-Principles Prediction of a Room-Temperature Ferromagnetic Janus VSSe Monolayer with Piezoelectricity, Ferroelasticity, and Large Valley Polarization. Nano Letters, 2019, 19, 1366-1370.	4.5	292
20	First-Principles Prediction of Metal-Free Magnetism and Intrinsic Half-Metallicity in Graphitic Carbon Nitride. Physical Review Letters, 2012, 108, 197207.	2.9	272
21	Understanding the Roles of Oxygen Vacancies in Hematiteâ€Based Photoelectrochemical Processes. Angewandte Chemie - International Edition, 2019, 58, 1030-1034.	7.2	268
22	Hybrid Graphene/Titania Nanocomposite: Interface Charge Transfer, Hole Doping, and Sensitization for Visible Light Response. Journal of Physical Chemistry Letters, 2011, 2, 894-899.	2.1	252
23	New Iron obalt Oxide Catalysts Promoting BiVO ₄ Films for Photoelectrochemical Water Splitting. Advanced Functional Materials, 2018, 28, 1802685.	7.8	248
24	Synergistic crystal facet engineering and structural control of WO3 films exhibiting unprecedented photoelectrochemical performance. Nano Energy, 2016, 24, 94-102.	8.2	243
25	In Situ Formation of Oxygen Vacancies Achieving Nearâ€Complete Charge Separation in Planar BiVO ₄ Photoanodes. Advanced Materials, 2020, 32, e2001385.	11.1	236
26	Single Molybdenum Atom Anchored on N-Doped Carbon as a Promising Electrocatalyst for Nitrogen Reduction into Ammonia at Ambient Conditions. Journal of Physical Chemistry C, 2018, 122, 16842-16847.	1.5	223
27	Graphene-like Two-Dimensional Ionic Boron with Double Dirac Cones at Ambient Condition. Nano Letters, 2016, 16, 3022-3028.	4.5	222
28	Moltenâ€5altâ€Mediated Synthesis of an Atomic Nickel Coâ€catalyst on TiO ₂ for Improved Photocatalytic H ₂ Evolution. Angewandte Chemie - International Edition, 2020, 59, 7230-7234.	7.2	221
29	Edgeâ€Rich Feâ^'N ₄ Active Sites in Defective Carbon for Oxygen Reduction Catalysis. Advanced Materials, 2020, 32, e2000966.	11.1	215
30	An Intrinsically Nonâ€flammable Electrolyte for Highâ€Performance Potassium Batteries. Angewandte Chemie - International Edition, 2020, 59, 3638-3644.	7.2	211
31	Structural and Electronic Properties of Layered Arsenic and Antimony Arsenide. Journal of Physical Chemistry C, 2015, 119, 6918-6922.	1.5	210
32	Dirac State in the FeB ₂ Monolayer with Graphene-Like Boron Sheet. Nano Letters, 2016, 16, 6124-6129.	4.5	200
33	Anti-fouling graphene-based membranes for effective water desalination. Nature Communications, 2018, 9, 683.	5.8	197
34	Transitionâ€Metal Single Atoms Anchored on Graphdiyne as Highâ€Efficiency Electrocatalysts for Water Splitting and Oxygen Reduction. Small Methods, 2019, 3, 1800419.	4.6	192
35	Rapid microwave-assisted synthesis of Mn3O4–graphene nanocomposite and its lithium storage properties. Journal of Materials Chemistry, 2012, 22, 3600.	6.7	183
36	First-principle studies of electronic structure and C-doping effect in boron nitride nanoribbon. Chemical Physics Letters, 2007, 447, 181-186.	1.2	180

#	Article	IF	CITATIONS
37	Strain engineering of selective chemical adsorption on monolayer MoS ₂ . Nanoscale, 2014, 6, 5156-5161.	2.8	177
38	Auxetic and Ferroelastic Borophane: A Novel 2D Material with Negative Possion's Ratio and Switchable Dirac Transport Channels. Nano Letters, 2016, 16, 7910-7914.	4.5	176
39	Dots versus Antidots: Computational Exploration of Structure, Magnetism, and Half-Metallicity in Boronâ^'Nitride Nanostructures. Journal of the American Chemical Society, 2009, 131, 17354-17359.	6.6	174
40	Hydrogenated borophene as a stable two-dimensional Dirac material with an ultrahigh Fermi velocity. Physical Chemistry Chemical Physics, 2016, 18, 27284-27289.	1.3	167
41	Tuning oxygen vacancies in two-dimensional iron-cobalt oxide nanosheets through hydrogenation for enhanced oxygen evolution activity. Nano Research, 2018, 11, 3509-3518.	5.8	167
42	Lithiumâ€Catalyzed Dehydrogenation of Ammonia Borane within Mesoporous Carbon Framework for Chemical Hydrogen Storage. Advanced Functional Materials, 2009, 19, 265-271.	7.8	156
43	Manipulating the Solvation Structure of Nonflammable Electrolyte and Interface to Enable Unprecedented Stability of Graphite Anodes beyond 2 Years for Safe Potassiumâ€ion Batteries. Advanced Materials, 2021, 33, e2006313.	11.1	155
44	Tuning the Intermolecular Electron Transfer of Low-Dimensional and Metal-Free BCN/C ₆₀ Electrocatalysts via Interfacial Defects for Efficient Hydrogen and Oxygen Electrochemistry. Journal of the American Chemical Society, 2021, 143, 1203-1215.	6.6	140
45	Mo-based 2D MOF as a highly efficient electrocatalyst for reduction of N ₂ to NH ₃ : a density functional theory study. Journal of Materials Chemistry A, 2019, 7, 14510-14518.	5.2	139
46	Activating Catalytic Inert Basal Plane of Molybdenum Disulfide to Optimize Hydrogen Evolution Activity via Defect Doping and Strain Engineering. Journal of Physical Chemistry C, 2016, 120, 16761-16766.	1.5	138
47	Metallic and Carbon Nanotube-Catalyzed Coupling of Hydrogenation in Magnesium. Journal of the American Chemical Society, 2007, 129, 15650-15654.	6.6	131
48	Computational screening of two-dimensional coordination polymers as efficient catalysts for oxygen evolution and reduction reaction. Journal of Catalysis, 2017, 352, 579-585.	3.1	130
49	Electronic and optical properties of lead-free hybrid double perovskites for photovoltaic and optoelectronic applications. Scientific Reports, 2019, 9, 718.	1.6	130
50	Highâ€Performance Perovskite Composite Electrocatalysts Enabled by Controllable Interface Engineering. Small, 2021, 17, e2101573.	5.2	128
51	Metal-free graphitic carbon nitride as mechano-catalyst for hydrogen evolution reaction. Journal of Catalysis, 2015, 332, 149-155.	3.1	127
52	Single tungsten atom supported on N-doped graphyne as a high-performance electrocatalyst for nitrogen fixation under ambient conditions. Physical Chemistry Chemical Physics, 2019, 21, 1546-1551.	1.3	126
53	Transition metal dichalcogenides bilayer single crystals by reverse-flow chemical vapor epitaxy. Nature Communications, 2019, 10, 598.	5.8	124
54	Atomically embedded asymmetrical dual-metal dimers on N-doped graphene for ultra-efficient nitrogen reduction reaction. Journal of Catalysis, 2020, 388, 77-83.	3.1	123

#	Article	IF	CITATIONS
55	A Directional Synthesis for Topological Defect in Carbon. CheM, 2020, 6, 2009-2023.	5.8	120
56	The Role of Ti as a Catalyst for the Dissociation of Hydrogen on a Mg(0001) Surface. Journal of Physical Chemistry B, 2005, 109, 18037-18041.	1.2	113
57	Tailoring the Interfacial Interactions of van der Waals 1T-MoS ₂ /C ₆₀ Heterostructures for High-Performance Hydrogen Evolution Reaction Electrocatalysis. Journal of the American Chemical Society, 2020, 142, 17923-17927.	6.6	112
58	Controllable CO2 electrocatalytic reduction via ferroelectric switching on single atom anchored In2Se3 monolayer. Nature Communications, 2021, 12, 5128.	5.8	110
59	A single boron atom doped boron nitride edge as a metal-free catalyst for N ₂ fixation. Physical Chemistry Chemical Physics, 2019, 21, 1110-1116.	1.3	107
60	C-BN Single-Walled Nanotubes from Hybrid Connection of BN/C Nanoribbons: Prediction by <i>ab initio</i> Density Functional Calculations. Journal of the American Chemical Society, 2009, 131, 1682-1683.	6.6	106
61	Hydrogen Spillover Mechanism on a Pd-Doped Mg Surface as Revealed by ab initio Density Functional Calculation. Journal of the American Chemical Society, 2007, 129, 10201-10204.	6.6	105
62	Carbon nanodot decorated graphitic carbon nitride: new insights into the enhanced photocatalytic water splitting from ab initio studies. Physical Chemistry Chemical Physics, 2015, 17, 31140-31144.	1.3	105
63	Widely tunable and anisotropic charge carrier mobility in monolayer tin(<scp>ii</scp>) selenide using biaxial strain: a first-principles study. Journal of Materials Chemistry C, 2017, 5, 1247-1254.	2.7	104
64	Computational Dissection of Two-Dimensional Rectangular Titanium Mononitride TiN: Auxetics and Promises for Photocatalysis. Nano Letters, 2017, 17, 4466-4472.	4.5	104
65	Gas sensing and capturing based on twoâ€dimensional layered materials: Overview from theoretical perspective. Wiley Interdisciplinary Reviews: Computational Molecular Science, 2018, 8, e1361.	6.2	101
66	Twoâ€Dimensional Boron Hydride Sheets: High Stability, Massless Dirac Fermions, and Excellent Mechanical Properties. Angewandte Chemie - International Edition, 2016, 55, 10292-10295.	7.2	100
67	Predicting Single-Layer Technetium Dichalcogenides (TcX ₂ , X = S, Se) with Promising Applications in Photovoltaics and Photocatalysis. ACS Applied Materials & Interfaces, 2016, 8, 5385-5392.	4.0	100
68	Single Pt atom decorated graphitic carbon nitride as an efficient photocatalyst for the hydrogenation of nitrobenzene into aniline. Nano Research, 2019, 12, 1817-1823.	5.8	100
69	Porous Polyethersulfone-Supported Zeolitic Imidazolate Framework Membranes for Hydrogen Separation. Journal of Physical Chemistry C, 2012, 116, 13264-13270.	1.5	96
70	Nanosheets Co ₃ O ₄ Interleaved with Graphene for Highly Efficient Oxygen Reduction. ACS Applied Materials & Interfaces, 2015, 7, 21373-21380.	4.0	96
71	Stable Copper Nanoparticle Photocatalysts for Selective Epoxidation of Alkenes with Visible Light. ACS Catalysis, 2017, 7, 4975-4985.	5.5	96
72	Mg-Based Nanocomposites with High Capacity and Fast Kinetics for Hydrogen Storage. Journal of Physical Chemistry B, 2006, 110, 11697-11703.	1.2	95

#	Article	IF	CITATIONS
73	Modelling carbon membranes for gas and isotope separation. Physical Chemistry Chemical Physics, 2013, 15, 4832.	1.3	95
74	Twoâ€Dimensional Boron Hydride Sheets: High Stability, Massless Dirac Fermions, and Excellent Mechanical Properties. Angewandte Chemie, 2016, 128, 10448-10451.	1.6	94
75	Understanding the activity and selectivity of single atom catalysts for hydrogen and oxygen evolution <i>via</i> ab initial study. Catalysis Science and Technology, 2018, 8, 996-1001.	2.1	94
76	An Unusual Red Carbon Nitride to Boost the Photoelectrochemical Performance of Wide Bandgap Photoanodes. Advanced Functional Materials, 2018, 28, 1805698.	7.8	94
77	Strong Coupling of MoS ₂ Nanosheets and Nitrogenâ€Doped Graphene for Highâ€Performance Pseudocapacitance Lithium Storage. Small, 2018, 14, e1704410.	5.2	89
78	Understanding the Roles of Oxygen Vacancies in Hematiteâ€Based Photoelectrochemical Processes. Angewandte Chemie, 2019, 131, 1042-1046.	1.6	89
79	Tailoring Crystal Structure of FA _{0.83} Cs _{0.17} PbI ₃ Perovskite Through Guanidinium Doping for Enhanced Performance and Tunable Hysteresis of Planar Perovskite Solar Cells. Advanced Functional Materials, 2019, 29, 1806479.	7.8	87
80	First principle studies of zigzag AlN nanoribbon. Chemical Physics Letters, 2009, 469, 183-185.	1.2	86
81	Dualâ€lonâ€Diffusion Induced Degradation in Leadâ€Free Cs ₂ AgBiBr ₆ Double Perovskite Solar Cells. Advanced Functional Materials, 2020, 30, 2002342.	7.8	86
82	Endohedral metallofullerenes (M@C60) as efficient catalysts for highly active hydrogen evolution reaction. Journal of Catalysis, 2017, 354, 231-235.	3.1	84
83	First-Principles Prediction of Spin-Polarized Multiple Dirac Rings in Manganese Fluoride. Physical Review Letters, 2017, 119, 016403.	2.9	84
84	2D–3D Mixed Organic–Inorganic Perovskite Layers for Solar Cells with Enhanced Efficiency and Stability Induced by <i>n</i> -Propylammonium Iodide Additives. ACS Applied Materials & Interfaces, 2019, 11, 29753-29764.	4.0	83
85	Spin-polarization and ferromagnetism of graphitic carbon nitride materials. Journal of Materials Chemistry C, 2013, 1, 6265.	2.7	82
86	Identifying Copper Vacancies and Their Role in the CuO Based Photocathode for Water Splitting. Angewandte Chemie - International Edition, 2019, 58, 17604-17609.	7.2	82
87	Asymmetrically Decorated, Doped Porous Graphene As an Effective Membrane for Hydrogen Isotope Separation. Journal of Physical Chemistry C, 2012, 116, 6672-6676.	1.5	81
88	Two-dimensional GeP ₃ as a high capacity electrode material for Li-ion batteries. Physical Chemistry Chemical Physics, 2017, 19, 25886-25890.	1.3	81
89	A density functional theory study on CO2 capture and activation by graphene-like boron nitride with boron vacancy. Catalysis Today, 2011, 175, 271-275.	2.2	80
90	Single layer lead iodide: computational exploration of structural, electronic and optical properties, strain induced band modulation and the role of spin–orbital-coupling. Nanoscale, 2015, 7, 15168-15174.	2.8	80

#	Article	IF	CITATIONS
91	Gradientâ€Concentration Design of Stable Core–Shell Nanostructure for Acidic Oxygen Reduction Electrocatalysis. Advanced Materials, 2020, 32, e2003493.	11.1	79
92	Electric field controlled CO ₂ capture and CO ₂ /N ₂ separation on MoS ₂ monolayers. Nanoscale, 2017, 9, 19-24.	2.8	78
93	Atomically Dispersed Heteronuclear Dualâ€Atom Catalysts: A New Rising Star in Atomic Catalysis. Small, 2022, 18, e2106091.	5.2	78
94	Carbon Dioxide Capture and Gas Separation on B ₈₀ Fullerene. Journal of Physical Chemistry C, 2014, 118, 2170-2177.	1.5	77
95	Electrochemical reduction of carbon dioxide on precise number of Fe atoms anchored graphdiyne. Journal of CO2 Utilization, 2020, 37, 272-277.	3.3	76
96	Predicting Two-Dimensional C ₃ B/C ₃ N van der Waals p–n Heterojunction with Strong Interlayer Electron Coupling and Enhanced Photocurrent. Journal of Physical Chemistry Letters, 2018, 9, 858-862.	2.1	74
97	Novel two-dimensional MOF as a promising single-atom electrocatalyst for CO2 reduction: A theoretical study. Applied Surface Science, 2020, 500, 143993.	3.1	74
98	Plasma-induced on-surface sulfur vacancies in NiCo ₂ S ₄ enhance the energy storage performance of supercapatteries. Journal of Materials Chemistry A, 2020, 8, 9278-9291.	5.2	73
99	Strong affinity of polysulfide intermediates to multi-functional binder for practical application in lithium–sulfur batteries. Nano Energy, 2016, 26, 722-728.	8.2	72
100	Hindered Formation of Photoinactive δ-FAPbI ₃ Phase and Hysteresis-Free Mixed-Cation Planar Heterojunction Perovskite Solar Cells with Enhanced Efficiency via Potassium Incorporation. Journal of Physical Chemistry Letters, 2018, 9, 2113-2120.	2.1	72
101	Two-Dimensional Titanium Carbonitride Mxene for High-Performance Sodium Ion Batteries. ACS Applied Nano Materials, 2018, 1, 6854-6863.	2.4	71
102	Metal-doped graphitic carbon nitride (g-C3N4) as selective NO2 sensors: A first-principles study. Applied Surface Science, 2018, 455, 1116-1122.	3.1	71
103	Single-atom supported on graphene grain boundary as an efficient electrocatalyst for hydrogen evolution reaction. Chemical Engineering Science, 2019, 194, 58-63.	1.9	71
104	Computation-Aided Design of Single-Atom Catalysts for One-Pot CO ₂ Capture, Activation, and Conversion. ACS Applied Materials & amp; Interfaces, 2018, 10, 36866-36872.	4.0	70
105	A water-dielectric capacitor using hydrated graphene oxide film. Journal of Materials Chemistry, 2012, 22, 21085.	6.7	68
106	Ab initio studies of hydrogen desorption from low index magnesium hydride surface. Surface Science, 2006, 600, 1854-1859.	0.8	67
107	Single Layer Bismuth Iodide: Computational Exploration of Structural, Electrical, Mechanical and Optical Properties. Scientific Reports, 2015, 5, 17558.	1.6	67
108	H ₂ purification by functionalized graphdiyne – role of nitrogen doping. Journal of Materials Chemistry A, 2015, 3, 6767-6771.	5.2	67

#	Article	IF	CITATIONS
109	Ultra-dense carbon defects as highly active sites for oxygen reduction catalysis. CheM, 2022, 8, 2715-2733.	5.8	66
110	Predicting Novel 2D MB ₂ (M = Ti, Hf, V, Nb, Ta) Monolayers with Ultrafast Dirac Transport Channel and Electron-Orbital Controlled Negative Poisson's Ratio. Journal of Physical Chemistry Letters, 2019, 10, 2567-2573.	2.1	65
111	Surfaceâ€Dependent Intermediate Adsorption Modulation on Iridiumâ€Modified Black Phosphorus Electrocatalysts for Efficient pHâ€Universal Water Splitting. Advanced Materials, 2021, 33, e2104638.	11.1	65
112	High capacity and reversible hydrogen storage on two dimensional C 2 N monolayer membrane. International Journal of Hydrogen Energy, 2018, 43, 9895-9901.	3.8	64
113	Controlling the Interfacial Charge Polarization of MOF-Derived 0D–2D vdW Architectures as a Unique Strategy for Bifunctional Oxygen Electrocatalysis. ACS Applied Materials & Interfaces, 2022, 14, 3919-3929.	4.0	63
114	A density functional theory study of CO2 and N2 adsorption on aluminium nitride single walled nanotubes. Journal of Materials Chemistry, 2010, 20, 10426.	6.7	62
115	Electrocatalytically Switchable CO ₂ Capture: First Principle Computational Exploration of Carbon Nanotubes with Pyridinic Nitrogen. ChemSusChem, 2014, 7, 435-441.	3.6	62
116	First-Principle Studies of the Formation and Diffusion of Hydrogen Vacancies in Magnesium Hydride. Journal of Physical Chemistry C, 2007, 111, 8360-8365.	1.5	61
117	Predicting a new class of metal-organic frameworks as efficient catalyst for bi-functional oxygen evolution/reduction reactions. Journal of Catalysis, 2018, 367, 206-211.	3.1	61
118	Versatile Single-Layer Sodium Phosphidostannate(II): Strain-Tunable Electronic Structure, Excellent Mechanical Flexibility, and an Ideal Gap for Photovoltaics. Journal of Physical Chemistry Letters, 2015, 6, 2682-2687.	2.1	60
119	Ultrathin Cobaltosic Oxide Nanosheets as an Effective Sulfur Encapsulation Matrix with Strong Affinity Toward Polysulfides. ACS Applied Materials & Interfaces, 2017, 9, 4320-4325.	4.0	59
120	Simplest MOF Units for Effective Photodriven Hydrogen Evolution Reaction. Journal of the American Chemical Society, 2018, 140, 9159-9166.	6.6	59
121	Reversible gas capture using a ferroelectric switch and 2D molecule multiferroics on the In ₂ Se ₃ monolayer. Journal of Materials Chemistry A, 2020, 8, 7331-7338.	5.2	59
122	Sodium and Lithium Storage Properties of Spray-Dried Molybdenum Disulfide-Graphene Hierarchical Microspheres. Scientific Reports, 2015, 5, 11989.	1.6	58
123	Atomically dispersed asymmetric Cu–B pair on 2D carbon nitride synergistically boosts the conversion of CO into C ₂ products. Journal of Materials Chemistry A, 2020, 8, 599-606.	5.2	58
124	Fabricating highly efficient heterostructured CuBi ₂ O ₄ photocathodes for unbiased water splitting. Journal of Materials Chemistry A, 2020, 8, 2498-2504.	5.2	57
125	Electronic Functionality in Graphene-Based Nanoarchitectures: Discovery and Design via First-Principles Modeling. Journal of Physical Chemistry Letters, 2011, 2, 73-80.	2.1	56
126	Van der Waals-corrected density functional theory: benchmarking for hydrogen–nanotube and nanotube–nanotube interactions. Nanotechnology, 2005, 16, 2118-2123.	1.3	55

#	Article	IF	CITATIONS
127	Catalytic Effects of Subsurface Carbon in the Chemisorption of Hydrogen on a Mg(0001) Surface:Â an Ab-initio Study. Journal of Physical Chemistry B, 2006, 110, 1814-1819.	1.2	55
128	Combined electrophoretic deposition–anodization method to fabricate reduced graphene oxide–TiO2 nanotube films. RSC Advances, 2012, 2, 8164.	1.7	55
129	Distorted Janus Transition Metal Dichalcogenides: Stable Two-Dimensional Materials with Sizable Band Gap and Ultrahigh Carrier Mobility. Journal of Physical Chemistry C, 2018, 122, 19153-19160.	1.5	55
130	Moltenâ€6altâ€Mediated Synthesis of an Atomic Nickel Co atalyst on TiO ₂ for Improved Photocatalytic H ₂ Evolution. Angewandte Chemie, 2020, 132, 7297-7301.	1.6	55
131	A zinc bromine "supercapattery―system combining triple functions of capacitive, pseudocapacitive and battery-type charge storage. Materials Horizons, 2020, 7, 495-503.	6.4	54
132	Adsorption of Carbon Dioxide and Nitrogen on Single-Layer Aluminum Nitride Nanostructures Studied by Density Functional Theory. Journal of Physical Chemistry C, 2010, 114, 7846-7849.	1.5	53
133	First-Principle Study of Adsorption of Hydrogen on Ti-Doped Mg(0001) Surface. Journal of Physical Chemistry B, 2006, 110, 21747-21750.	1.2	52
134	Gas Protection of Two-Dimensional Nanomaterials from High-Energy Impacts. Scientific Reports, 2016, 6, 35532.	1.6	52
135	Computational screening of MN ₄ (M = Ti–Cu) based metal organic frameworks for CO ₂ reduction using the d-band centre as a descriptor. Nanoscale, 2020, 12, 6188-6194.	2.8	52
136	Novel Excitonic Solar Cells in Phosphorene–TiO ₂ Heterostructures with Extraordinary Charge Separation Efficiency. Journal of Physical Chemistry Letters, 2016, 7, 1880-1887.	2.1	51
137	In-plane graphene/boron-nitride heterostructures as an efficient metal-free electrocatalyst for the oxygen reduction reaction. Nanoscale, 2016, 8, 14084-14091.	2.8	51
138	Versatile two-dimensional silicon diphosphide (SiP ₂) for photocatalytic water splitting. Nanoscale, 2018, 10, 6369-6374.	2.8	51
139	Firstâ€Principles Study of Electrocatalytically Reversible CO ₂ Capture on Grapheneâ€ike C ₃ N. ChemPhysChem, 2018, 19, 2788-2795.	1.0	51
140	Silicon-doped graphene edges: an efficient metal-free catalyst for the reduction of CO ₂ into methanol and ethanol. Catalysis Science and Technology, 2019, 9, 6800-6807.	2.1	51
141	Predicting a new phase (Tâ \in 2â \in 2) of two-dimensional transition metal di-chalcogenides and strain-controlled topological phase transition. Nanoscale, 2016, 8, 4969-4975.	2.8	50
142	Ab initio atomistic insights into lead-free formamidinium based hybrid perovskites for photovoltaics and optoelectronics. Computational Materials Science, 2019, 169, 109118.	1.4	50
143	Reversible Intercalation of Multivalent Al ³⁺ Ions into Potassiumâ€Rich Cryptomelane Nanowires for Aqueous Rechargeable Alâ€ion Batteries. ChemSusChem, 2019, 12, 3753-3760.	3.6	50
144	Prediction of room-temperature ferromagnetism and large perpendicular magnetic anisotropy in a planar hypercoordinate FeB ₃ monolayer. Nanoscale Horizons, 2021, 6, 43-48.	4.1	50

#	Article	IF	CITATIONS
145	Leaf-inspired design of mesoporous Sb2S3/N-doped Ti3C2Tx composite towards fast sodium storage. Science China Chemistry, 2021, 64, 964-973.	4.2	50
146	Doped phosphorene for hydrogen capture: A DFT study. Applied Surface Science, 2018, 433, 249-255.	3.1	48
147	First-principles screening of novel ferroelectric MXene phases with a large piezoelectric response and unusual auxeticity. Nanoscale, 2020, 12, 21291-21298.	2.8	48
148	Computational Design and Experimental Validation of the Optimal Bimetal-Doped SrCoO _{3â^î} Perovskite as Solid Oxide Fuel Cell Cathode. Journal of the American Chemical Society, 2021, 143, 9507-9514.	6.6	48
149	Insights into the nature of the coupling interactions between uracil corrosion inhibitors and copper: A DFT and molecular dynamics study. Corrosion Science, 2012, 61, 101-110.	3.0	47
150	Moleculeâ€Induced Conformational Change in Boron Nitride Nanosheets with Enhanced Surface Adsorption. Advanced Functional Materials, 2016, 26, 8202-8210.	7.8	47
151	WO ₃ nanolayer coated 3D-graphene/sulfur composites for high performance lithium/sulfur batteries. Journal of Materials Chemistry A, 2019, 7, 4596-4603.	5.2	47
152	Development of cross-linked dextrin as aqueous binders for silicon based anodes. Journal of Power Sources, 2020, 450, 227671.	4.0	47
153	Stacking-Dependent Interlayer Magnetic Coupling in 2D Crl ₃ /CrGeTe ₃ Nanostructures for Spintronics. ACS Applied Nano Materials, 2020, 3, 1282-1288.	2.4	47
154	Graphene-covered perovskites: an effective strategy to enhance light absorption and resist moisture degradation. RSC Advances, 2015, 5, 82346-82350.	1.7	43
155	Rhombohedral Lanthanum Manganite: A New Class of Dirac Half-Metal with Promising Potential in Spintronics. ACS Applied Materials & Interfaces, 2018, 10, 36088-36093.	4.0	43
156	Galvanic replacement of liquid metal galinstan with Pt for the synthesis of electrocatalytically active nanomaterials. Nanoscale, 2019, 11, 9705-9715.	2.8	43
157	Charge―and Electricâ€Fieldâ€Controlled Switchable Carbon Dioxide Capture and Gas Separation on a C ₂ N Monolayer. Energy Technology, 2018, 6, 205-212.	1.8	42
158	An amorphous dual action electrocatalyst based on oxygen doped cobalt sulfide for the hydrogen and oxygen evolution reactions. RSC Advances, 2017, 7, 54995-55004.	1.7	41
159	Conduction-band valley spin splitting in single-layer H- <mml:math xmlns:mml="http://www.w3.org/1998/Math/MathML"> <mml:mrow> <mml:mi mathvariant="normal">T <mml:msub> <mml:mi mathvariant="normal">I <mml:msub> <mml:mi mathvariant="normal">I <mml:msub> </mml:msub> <mml:msub> <mml:mi< td=""><td>1.1</td><td>41</td></mml:mi<></mml:msub></mml:mi </mml:msub></mml:mi </mml:msub></mml:mi </mml:mrow></mml:math 	1.1	41
160	mathvariant="normal">O. Physical Review B, 2018, 97, . Thermal Reductive Perforation of Graphene Cathode for Highâ€Performance Aluminumâ€Ion Batteries. Advanced Functional Materials, 2021, 31, 2010569.	7.8	41
161	Graphyne and Graphdiyne: Versatile Catalysts for Dehydrogenation of Light Metal Complex Hydrides. Journal of Physical Chemistry C, 2013, 117, 21643-21650.	1.5	40
162	CO2 capture and gas separation on boron carbon nanotubes. Chemical Physics Letters, 2013, 575, 59-66.	1.2	40

#	Article	IF	CITATIONS
163	Modelling CO 2 adsorption and separation on experimentally-realized B 40 fullerene. Computational Materials Science, 2015, 108, 38-41.	1.4	40
164	Predicting a graphene-like WB4 nanosheet with a double Dirac cone, an ultra-high Fermi velocity and significant gap opening by spin–orbit coupling. Physical Chemistry Chemical Physics, 2017, 19, 5449-5453.	1.3	40
165	Integrating SnS ₂ Quantum Dots with Nitrogen-Doped Ti ₃ C ₂ T _{<i>x</i>} MXene Nanosheets for Robust Sodium Storage Performance. ACS Applied Energy Materials, 2021, 4, 846-854.	2.5	40
166	Adsorption behavior of CO2 on pristine and doped phosphorenes: A dispersion corrected DFT study. Journal of CO2 Utilization, 2018, 24, 463-470.	3.3	39
167	Grafting Cobalt Diselenide on Defective Graphene for Enhanced Oxygen Evolution Reaction. IScience, 2018, 7, 145-153.	1.9	39
168	Ultralarge interlayer distance and C,N-codoping enable superior sodium storage capabilities of MoS2 nanoonions. Chemical Engineering Journal, 2019, 378, 122249.	6.6	39
169	Boron Radicals Identified as the Source of the Unexpected Catalysis by Boron Nitride Nanosheets. ACS Nano, 2019, 13, 1394-1402.	7.3	39
170	Plasmonic nanostructures to enhance catalytic performance of zeolites under visible light. Scientific Reports, 2014, 4, 3805.	1.6	37
171	Two-dimensional ferroelectric topological insulators in functionalized atomically thin bismuth layers. Physical Review B, 2018, 97, .	1.1	37
172	Transition Metal Diborides: A New Type of Highâ€performance Electrocatalysts for Nitrogen Reduction. ChemCatChem, 2019, 11, 2624-2633.	1.8	37
173	2D/2D Black Phosphorus/Nickel Hydroxide Heterostructures for Promoting Oxygen Evolution via Electronic Structure Modulation and Surface Reconstruction. Advanced Energy Materials, 2022, 12, .	10.2	37
174	2D atomic crystal molecular superlattices by soft plasma intercalation. Nature Communications, 2020, 11, 5960.	5.8	36
175	Tetragonal bismuth bilayer: a stable and robust quantum spin hall insulator. 2D Materials, 2015, 2, 045010.	2.0	34
176	Defective Graphene on the Transition-Metal Surface: Formation of Efficient Bifunctional Catalysts for Oxygen Evolution/Reduction Reactions in Alkaline Media. ACS Applied Materials & Interfaces, 2019, 11, 17410-17415.	4.0	34
177	Mo-doped boron nitride monolayer as a promising single-atom electrocatalyst for CO ₂ conversion. Beilstein Journal of Nanotechnology, 2019, 10, 540-548.	1.5	34
178	Synergistic trifunctional electrocatalysis of pyridinic nitrogen and single transition-metal atoms anchored on pyrazine-modified graphdiyne. Science Bulletin, 2020, 65, 995-1002.	4.3	34
179	Nitrateâ€ŧoâ€Ammonia Conversion at an InSnâ€Enriched Liquidâ€Metal Electrode. Angewandte Chemie - International Edition, 2022, 61, .	7.2	34
180	Vertically-aligned carbon nanotube membranes for hydrogen separation. RSC Advances, 2012, 2, 5329.	1.7	33

#	Article	IF	CITATIONS
181	Carbon–Phosphorus Bonds-Enriched 3D Graphene by Self-Sacrificing Black Phosphorus Nanosheets for Elevating Capacitive Lithium Storage. ACS Applied Materials & Interfaces, 2020, 12, 21720-21729.	4.0	33
182	Computational screening of single-atom alloys TM@Ru(0001) for enhanced electrochemical nitrogen reduction reaction. Journal of Materials Chemistry A, 2022, 10, 6204-6215.	5.2	33
183	Adina Rubellaâ€Like Microsized SiO@Nâ€Doped Carbon Grafted with Nâ€Doped Carbon Nanotubes as Anodes for Highâ€Performance Lithium Storage. Small Science, 2022, 2, .	5.8	33
184	<i>In silico</i> engineering of grapheneâ€based van der Waals heterostructured nanohybrids for electronics and energy applications. Wiley Interdisciplinary Reviews: Computational Molecular Science, 2016, 6, 551-570.	6.2	32
185	Plasma modification of a Ni based metal–organic framework for efficient hydrogen evolution. Journal of Materials Chemistry A, 2019, 7, 8129-8135.	5.2	32
186	Potassium Doping to Enhance Green Photoemission of Lightâ€Emitting Diodes Based on CsPbBr ₃ Perovskite Nanocrystals. Advanced Optical Materials, 2020, 8, 2000742.	3.6	32
187	Nanostructure Shape-Effects in ZnO heterogeneous photocatalysis. Journal of Colloid and Interface Science, 2022, 606, 588-599.	5.0	32
188	A computational study of carbon dioxide adsorption on solid boron. Physical Chemistry Chemical Physics, 2014, 16, 12695-12702.	1.3	31
189	Multiferroic and Ferroic Topological Order in Ligand-Functionalized Germanene and Arsenene. Physical Review Applied, 2018, 10, .	1.5	31
190	Decorating platinum on nitrogen-doped graphene sheets: Control of the platinum particle size distribution for improved photocatalytic H2 generation. Chemical Engineering Science, 2019, 194, 85-93.	1.9	31
191	Group 14 element-based non-centrosymmetric quantum spin Hall insulators with large bulk gap. Nano Research, 2015, 8, 3412-3420.	5.8	30
192	The catalytic role of an isolated-Ti atom in the hydrogenation of Ti-doped Al(001) surface: An ab initio density functional theory calculation. Chemical Physics Letters, 2007, 450, 80-85.	1.2	29
193	Non-covalent surface modification of boron nitride nanotubes for enhanced catalysis. Chemical Communications, 2014, 50, 225-227.	2.2	29
194	Neutral and charged boron-doped fullerenes for CO ₂ adsorption. Beilstein Journal of Nanotechnology, 2014, 5, 413-418.	1.5	29
195	Borophene: A Metalâ€free and Metallic Electrocatalyst for Efficient Converting CO ₂ into CH ₄ . ChemCatChem, 2020, 12, 1483-1490.	1.8	29
196	Remarkably improved oxygen evolution reaction activity of cobalt oxides by an Fe ion solution immersion process. Inorganic Chemistry Frontiers, 2020, 7, 3327-3339.	3.0	29
197	Dimensionality-Controlled Surface Passivation for Enhancing Performance and Stability of Perovskite Solar Cells via Triethylenetetramine Vapor. ACS Applied Materials & Interfaces, 2020, 12, 6651-6661.	4.0	29
198	Electric-controlled half-metallicity in magnetic van der Waals heterobilayer. Journal of Materials Chemistry C, 2020, 8, 7034-7040.	2.7	29

#	Article	IF	CITATIONS
199	Carbon-coated MoS2 nanosheets@CNTs-Ti3C2 MXene quaternary composite with the superior rate performance for sodium-ion batteries. Journal of Materials Science and Technology, 2022, 100, 101-109.	5.6	29
200	Silicene catalysts for CO ₂ hydrogenation: the number of layers controls selectivity. Nanoscale, 2019, 11, 7734-7743.	2.8	28
201	Cobalt porphyrin supported on graphene/Ni (111) surface: Enhanced oxygen evolution/reduction reaction and the role of electron coupling. Catalysis Today, 2020, 351, 113-118.	2.2	28
202	Highly stable two-dimensional gold selenide with large in-plane anisotropy and ultrahigh carrier mobility. Nanoscale Horizons, 2020, 5, 366-371.	4.1	28
203	The role of V2O5 on the dehydrogenation and hydrogenation in magnesium hydride: An <i>ab initio</i> study. Applied Physics Letters, 2008, 92, .	1.5	27
204	Single Transition Metal Atom-Doped Graphene Supported on a Nickel Substrate: Enhanced Oxygen Reduction Reactions Modulated by Electron Coupling. Journal of Physical Chemistry C, 2019, 123, 3703-3710.	1.5	27
205	<pre><mmi:math xmins:mmi="http://www.w3.org/1998/Math/Math/Math/Math/Math/Math/Math/Math</td"><td>mml<mark>an</mark>row</td><td>><!--<b-->¤ml:msup</td></mmi:math></pre>	mml <mark>an</mark> row	> <b ¤ml:msup
206	carbon monoxide into repropanol. Journal of Catalysis, 2020, 382, 49-56. Computational Screening of Transition Metal–Phthalocyanines for the Electrochemical Reduction of Carbon Dioxide. Journal of Physical Chemistry C, 2020, 124, 7708-7715.	1.5	27
207	Theoretical insights into the performance of single and double transition metal atoms doped on N-graphenes for N2 electroreduction. Applied Surface Science, 2021, 537, 148012.	3.1	27
208	Band inversion and topological aspects in a TiNI monolayer. Physical Chemistry Chemical Physics, 2016, 18, 22154-22159.	1.3	26
209	Predicting New Two-Dimensional Pd ₃ (PS ₄) ₂ as an Efficient Photocatalyst for Water Splitting. Journal of Physical Chemistry C, 2018, 122, 21927-21932.	1.5	26
210	Tunable magnetic anisotropy in 2D magnets <i>via</i> molecular adsorption. Journal of Materials Chemistry C, 2020, 8, 14948-14953.	2.7	26
211	Highly compact and uniform CH3NH3Sn0.5Pb0.5I3 films for efficient panchromatic planar perovskite solar cells. Science Bulletin, 2016, 61, 1558-1562.	4.3	25
212	Boosting oxygen reduction and hydrogen evolution at the edge sites of a web-like carbon nanotube-graphene hybrid. Carbon, 2016, 107, 739-746.	5.4	25
213	Synthesis of biphenyl bridged dendritic mesoporous organosilica with extremely high adsorption of pyrene. Journal of Materials Chemistry A, 2019, 7, 12029-12037.	5.2	25
214	Strain engineering of selective chemical adsorption on monolayer black phosphorous. Applied Surface Science, 2020, 503, 144033.	3.1	25
215	Ultrasmall SnO ₂ nanocrystals sandwiched into polypyrrole and Ti ₃ C ₂ T _x MXene for highly effective sodium storage. Materials Chemistry Frontiers, 2021, 5, 825-833.	3.2	25
216	Techniques enabling inorganic materials into wearable fiber/yarn and flexible lithium-ion batteries. Energy Storage Materials, 2021, 43, 62-84.	9.5	25

#	Article	IF	CITATIONS
217	Formation of Single-Walled Carbon Nanotube via the Interaction of Graphene Nanoribbons:  Ab Initio Density Functional Calculations. Nano Letters, 2007, 7, 3349-3354.	4.5	24
218	Theoretical study of two states reactivity of methane activation on iron atom and iron dimer. Fuel, 2012, 96, 291-297.	3.4	24
219	Ab initio study of two-dimensional PdPS as an ideal light harvester and promising catalyst for hydrogen evolution reaction. Materials Today Energy, 2018, 7, 136-140.	2.5	24
220	Growth of MoS ₂ Nanoflowers with Expanded Interlayer Distance onto Nâ€Doped Graphene for Reversible Lithium Storage. ChemElectroChem, 2018, 5, 2263-2270.	1.7	24
221	Recent progress on the prediction of two-dimensional materials using CALYPSO. Chinese Physics B, 2019, 28, 107306.	0.7	24
222	Multiferroic decorated Fe ₂ O ₃ monolayer predicted from first principles. Nanoscale, 2020, 12, 14847-14852.	2.8	24
223	Nitrogen removal from natural gas using solid boron: A first-principles computational study. Fuel, 2013, 109, 575-581.	3.4	23
224	Strained graphitic carbon nitride for hydrogen purification. Journal of Membrane Science, 2017, 528, 201-205.	4.1	23
225	Visible light-driven selective hydrogenation of unsaturated aromatics in an aqueous solution by direct photocatalysis of Au nanoparticles. Catalysis Science and Technology, 2018, 8, 726-734.	2.1	23
226	Tuning CO binding strength <i>via</i> engineering the copper/borophene interface for highly efficient conversion of CO into ethanol. Journal of Materials Chemistry A, 2021, 9, 13192-13199.	5.2	23
227	The effect of Fe doping on adsorption of CO ₂ /N ₂ within carbon nanotubes: a density functional theory study with dispersion corrections. Nanotechnology, 2009, 20, 375701.	1.3	22
228	Charge carrier exchange at chemically modified graphene edges: a density functional theory study. Journal of Materials Chemistry, 2012, 22, 8321.	6.7	22
229	How to achieve maximum charge carrier loading on heteroatom-substituted graphene nanoribbon edges: density functional theory study. Journal of Materials Chemistry, 2012, 22, 13751.	6.7	22
230	Chemically modified ribbon edge stimulated H2 dissociation: a first-principles computational study. Physical Chemistry Chemical Physics, 2013, 15, 8054.	1.3	22
231	Unravelling the Reaction Mechanisms of N ₂ Fixation on Molybdenum Nitride: A Full DFT Study from the Pristine Surface to Heteroatom Anchoring. ChemSusChem, 2021, 14, 3257-3266.	3.6	22
232	Interaction of Water with the Fluorine-Covered Anatase TiO ₂ (001) Surface. Journal of Physical Chemistry C, 2011, 115, 17092-17096.	1.5	21
233	Charged-Controlled Separation of Nitrogen from Natural Gas Using Boron Nitride Fullerene. Journal of Physical Chemistry C, 2014, 118, 30006-30012.	1.5	21
234	Predicting multiple Dirac-cones and ultrahigh Fermi velocity in perovskite <i>R</i> 3Ì,, <i>c</i> phase LaCuO ₃ . Journal of Materials Chemistry C, 2018, 6, 6132-6137.	2.7	21

#	Article	IF	CITATIONS
235	Silicon Nanocages for Selective Carbon Dioxide Conversion under Visible Light. Journal of Physical Chemistry C, 2019, 123, 9973-9980.	1.5	21
236	Tuning band alignment and optical properties of 2D van der Waals heterostructure via ferroelectric polarization switching. Frontiers of Physics, 2020, 15, 1.	2.4	20
237	Boron-rich boron nitride nanomaterials as efficient metal-free catalysts for converting CO2 into valuable fuel. Applied Surface Science, 2021, 555, 149652.	3.1	20
238	Hydrogen-Intercalated 2D Magnetic Bilayer: Controlled Magnetic Phase Transition and Half-Metallicity via Ferroelectric Switching. ACS Applied Materials & Interfaces, 2022, 14, 1800-1806.	4.0	20
239	Theoretical Study of a Novel WSi ₂ N ₄ /MoSi ₂ N ₄ Heterostructure with Ultrafast Carrier Transport. Journal of Physical Chemistry C, 2022, 126, 11380-11388.	1.5	20
240	A theoretical insight into a feasible strategy for the fabrication of borophane. Physical Chemistry Chemical Physics, 2018, 20, 16216-16221.	1.3	19
241	B80 Fullerene: A Promising Metal-Free Photocatalyst for Efficient Conversion of CO2 to HCOOH. Journal of Physical Chemistry C, 2019, 123, 24193-24199.	1.5	19
242	The effect of ethylene-amine ligands enhancing performance and stability of perovskite solar cells. Journal of Power Sources, 2020, 463, 228210.	4.0	19
243	Methane activation on Fe4 cluster: A density functional theory study. Chemical Physics Letters, 2012, 550, 41-46.	1.2	18
244	Insights into the Mechanism of the Reaction between Tetrachloroâ€ <i>pâ€</i> Benzoquinone and Hydrogen Peroxide and their Implications in the Catalytic Role of Water Molecules in Producing the Hydroxyl Radial. ChemPhysChem, 2013, 14, 2737-2743.	1.0	18
245	Substantial Band-Gap Tuning and a Strain-Controlled Semiconductor to Gapless/Band-Inverted Semimetal Transition in Rutile Lead/Stannic Dioxide. ACS Applied Materials & Interfaces, 2016, 8, 25667-25673.	4.0	18
246	Density Functional Theory Investigation of Carbon Dots as Holeâ€transport Material in Perovskite Solar Cells. ChemPhysChem, 2018, 19, 3018-3023.	1.0	18
247	First-principles study of a Mn-doped <mml:math xmlns:mml="http://www.w3.org/1998/Math/MathML"> <mml:mrow> <mml:msub> <mml:mi>In </mml:mi> <mml:mi monolayer: Coexistence of ferromagnetism and ferroelectricity with robust half-metallicity and enhanced polarization. Physical Review B. 2020, 102</mml:mi </mml:msub></mml:mrow></mml:math 	>21.1	:mn>18
248	Two-dimensional vanadium tetrafluoride with antiferromagnetic ferroelasticity and bidirectional negative Poisson's ratio. Journal of Materials Chemistry C, 2021, 9, 95-100.	2.7	18
249	First-Principles Study of the Enhanced Magnetic Anisotropy and Transition Temperature in a CrSe ₂ Monolayer via Hydrogenation. ACS Applied Electronic Materials, 2022, 4, 3240-3245.	2.0	18
250	Addition of diazomethane to armchair single-walled carbon nanotubes and their reaction sequences: A computational study. Chemical Physics Letters, 2007, 436, 218-223.	1.2	17
251	2D boron dichalcogenides from the substitution of Mo with ionic B ₂ pair in MoX ₂ (X = S, Se and Te): high stability, large excitonic effect and high charge carrier mobility. Journal of Materials Chemistry C, 2019, 7, 1651-1658.	2.7	17
252	Metalâ€free graphene/boron nitride heterointerface for CO ₂ reduction: Surface curvature controls catalytic activity and selectivity. EcoMat, 2020, 2, e12013.	6.8	17

#	Article	IF	CITATIONS
253	Graphynes as emerging 2D-platforms for electronic and energy applications: a computational perspective. Materials Chemistry Frontiers, 2021, 5, 6392-6412.	3.2	17
254	Wavelength-Specific Product Desorption as a Key to Raising Nitrile Yield of Primary Alcohol Ammoxidation over Illuminated Pd Nanoparticles. ACS Catalysis, 2022, 12, 2280-2289.	5.5	17
255	Synthesis, structural analysis, and thermal decomposition studies of [(NH3)2BH2]B3H8. RSC Advances, 2013, 3, 7460.	1.7	16
256	Theoretical discovery of Dirac half metal in experimentally synthesized two dimensional metal semiquinoid frameworks. Journal of Materials Chemistry C, 2019, 7, 5792-5796.	2.7	16
257	An Intrinsically Nonâ€flammable Electrolyte for Highâ€Performance Potassium Batteries. Angewandte Chemie, 2020, 132, 3667-3673.	1.6	16
258	In-situ conversion growth of carbon-coated MoS2/N-doped carbon nanotubes as anodes with superior capacity retention for sodium-ion batteries. Journal of Materials Science and Technology, 2022, 102, 8-15.	5.6	16
259	Cobalt-doped cadmium selenide colloidal nanowires. Chemical Communications, 2011, 47, 11894.	2.2	15
260	Enhanced hydrogen separation by vertically-aligned carbon nanotube membranes with zeolite imidazolate frameworks as a selective layer. RSC Advances, 2012, 2, 11793.	1.7	15
261	Field-effect transistors fabricated from diluted magnetic semiconductor colloidal nanowires. Nanoscale, 2012, 4, 1263.	2.8	15
262	H ₂ S Sensing and Splitting on Atomâ€Functionalized Carbon Nanotubes: A Theoretical Study. Advanced Theory and Simulations, 2018, 1, 1700033.	1.3	15
263	Direct conversion of metal organic frameworks into ultrafine phosphide nanocomposites in multicomponent plasma for wide pH hydrogen evolution. Journal of Materials Chemistry A, 2020, 8, 10402-10408.	5.2	15
264	High capacity and mobility in germanium sulfide/graphene (GeS/Gr) van der Waals heterostructure as anode materials for sodium–ion batteries: A first-principles investigation. Applied Surface Science, 2021, 536, 147779.	3.1	15
265	Prediction of two-dimensional ferroelectric metal Mxenes. Journal of Materials Chemistry C, 2021, 9, 11343-11348.	2.7	15
266	B-incorporated, N-doped hierarchically porous carbon nanosheets as anodes for boosted potassium storage capability. Chinese Chemical Letters, 2022, 33, 480-485.	4.8	15
267	Revealing the Potential of Ternary Medium-Entropy Alloys as Exceptional Electrocatalysts toward Nitrogen Reduction: An Example of Heusler Alloys. ACS Applied Materials & Interfaces, 2022, 14, 15235-15242.	4.0	15
268	High-mobility anisotropic transport in few-layer γ-B ₂₈ films. Nanoscale, 2016, 8, 20111-20117.	2.8	14
269	Computational exploration of two-dimensional silicon diarsenide and germanium arsenide for photovoltaic applications. Beilstein Journal of Nanotechnology, 2018, 9, 1247-1253.	1.5	14
270	Unlocking the potential of ruthenium catalysts for nitrogen fixation with subsurface oxygen. Journal of Materials Chemistry A, 2021, 9, 6575-6582.	5.2	14

#	Article	IF	CITATIONS
271	Purely one-dimensional ferroelectricity and antiferroelectricity from van der Waals niobium oxide trihalides. Npj Computational Materials, 2021, 7, .	3.5	14
272	Pumpkin-like MoP-MoS2@Aspergillus niger spore-derived N-doped carbon heterostructure for enhanced potassium storage. Journal of Energy Chemistry, 2022, 72, 479-486.	7.1	14
273	Strain Mediated Bandgap Reduction, Light Spectrum Broadening, and Carrier Mobility Enhancement of Methylammonium Lead/Tin Iodide Perovskites. Particle and Particle Systems Characterization, 2017, 34, 1600288.	1.2	13
274	Versatile two-dimensional stanene-based membrane for hydrogen purification. International Journal of Hydrogen Energy, 2017, 42, 5577-5583.	3.8	13
275	Two-dimensional heterojunction SnS2/SnO2 photoanode with excellent photoresponse up to near infrared region. Solar Energy Materials and Solar Cells, 2020, 207, 110342.	3.0	13
276	The importance of atomic charge distributions of solid boron material in N2 electrochemical reduction. Applied Surface Science, 2020, 526, 146606.	3.1	13
277	Intrinsic Ultrahigh Negative Poisson's Ratio in Two-Dimensional Ferroelectric ABP ₂ X ₆ Materials. Wuli Huaxue Xuebao/ Acta Physico - Chimica Sinica, 2019, 35, 1128-1133.	2.2	13
278	Vacancy mediated desorption of hydrogen from a sodium alanate surface: An ab initio spin-polarized study. Applied Physics Letters, 2007, 90, 143119.	1.5	12
279	Computational study of methyl derivatives of ammonia borane for hydrogen storage. Physical Chemistry Chemical Physics, 2008, 10, 6104.	1.3	12
280	Surface plasmon-enhanced zeolite catalysis under light irradiation and its correlation with molecular polarity of reactants. Chemical Communications, 2014, 50, 13893-13895.	2.2	12
281	Controllable Polarization and Doping in Ferroelectric In ₂ Se ₃ Monolayers and Heterobilayers via Intrinsic Defect Engineering. Journal of Physical Chemistry C, 2021, 125, 24648-24654.	1.5	12
282	Kâ€Functionalized Carbon Quantum Dotsâ€Induced Interface Assembly of Carbon Nanocages for Ultrastable Potassium Storage Performance. Small Methods, 2022, 6, e2101627.	4.6	12
283	Prediction of a large-gap quantum-spin-Hall insulator: Diamond-like GaBi bilayer. Nano Research, 2015, 8, 3823-3829.	5.8	11
284	First-principles prediction of polar half-metallicity and out-of-plane piezoelectricity in two-dimensional quintuple layered cobalt selenide. Journal of Materials Chemistry C, 2021, 9, 12046-12050.	2.7	11
285	First-principles prediction of ferroelasticity tuned anisotropic auxeticity and carrier mobility in two-dimensional AgO. Journal of Materials Chemistry C, 2021, 9, 3155-3160.	2.7	11
286	Vacancy engineering of oxidized Nb2CTx MXenes for a biased nitrogen fixation. Green Energy and Environment, 2023, 8, 1185-1194.	4.7	11
287	Green ammonia synthesis using CeO ₂ /RuO ₂ nanolayers on vertical graphene catalyst <i>via</i> electrochemical route in alkaline electrolyte. Nanoscale, 2022, 14, 1395-1408.	2.8	11
288	Role of Lithium Vacancies in Accelerating the Dehydrogenation Kinetics on a LiBH ₄ (010) Surface:  An Ab Initio Study. Journal of Physical Chemistry C, 2007, 111, 12124-12128.	1.5	10

#	Article	IF	CITATIONS
289	Rhodium-molybdenum oxide electrocatalyst with dual active sites for electrochemical ammonia synthesis under neutral pH condition. Journal of Electroanalytical Chemistry, 2021, 896, 115157.	1.9	10
290	Coupling Fe3O4/Fe1-xS@Carbon with carbon-coated MoS2 nanosheets as a superior anode for sodium-ion batteries. Chemical Engineering Journal, 2022, 427, 131652.	6.6	10
291	Impact induced chemisorption of C20 isomers on diamond (001)–(2×1) surface. Chemical Physics Letters, 2001, 344, 270-276.	1.2	9
292	First Principle Study of Hydrogenation of MgB ₂ : An Important Step Toward Reversible Hydrogen Storage in the Coupled LiBH ₄ /MgH ₂ System. Journal of Nanoscience and Nanotechnology, 2009, 9, 4388-4391.	0.9	9
293	Calculations of helium separation via uniform pores of stanene-based membranes. Beilstein Journal of Nanotechnology, 2015, 6, 2470-2476.	1.5	9
294	First principles study of trirutile magnesium bismuth oxide: Ideal bandgap for photovoltaics, strain-mediated band-inversion and semiconductor-to-semimetal transition. Computational Materials Science, 2018, 149, 158-161. //www.w3.org/1998/Math/Math/M. *>cmmtmi	1.4	9
295	mathvariant="script">PT -symmetry-protected Dirac states in strain-induced hidden <mml:math xmlns:mml="http://www.w3.org/1998/Math/MathML"><mml:mrow><mml:mi>Mo</mml:mi><mml:msub><mml:m mathvariant="normal">S<mml:mn>2</mml:mn></mml:m </mml:msub></mml:mrow></mml:math 	i ^{1.1}	9
296	monolayer. Physical Review B, 2019, 100, Solvent Effect on Supramolecular Self-Assembly of Chlorophylls a on Chemically Reduced Graphene Oxide. Langmuir, 2020, 36, 13575-13582.	1.6	9
297	Single Copper Atoms Supported on ZnS as an Efficient Catalyst for Electrochemical Reduction of CO to CH ₃ OH. ChemNanoMat, 2020, 6, 1806-1811.	1.5	9
298	Bandstructure engineering in 2D materials using Ferroelectric materials. Applied Surface Science, 2020, 513, 145817.	3.1	9
299	Exploring Aluminumâ€ion Insertion into Magnesiumâ€Doped Manjiroite (MnO ₂) Nanorods in Aqueous Solution. ChemElectroChem, 2021, 8, 1048-1054.	1.7	9
300	Understanding the roles of carbon in carbon/g-C3N4 based photocatalysts for H2 evolution. Nano Research, 0, , 1.	5.8	9
301	Free-radical gases on two-dimensional transition-metal disulfides (XS ₂ , X = Mo/W): robust half-metallicity for efficient nitrogen oxide sensors. Beilstein Journal of Nanotechnology, 2018, 9, 1641-1646.	1.5	8
302	Sn ²⁺ -Regulated Synthesis of a Bone-like Fe ₃ O ₄ @N-Doped Carbon Composite as the Anode for High-Performance Lithium Storage. ACS Applied Energy Materials, 2021, 4, 3785-3793.	2.5	8
303	Co Nanoparticles Encapsulated in Nâ€Đoped Carbon Nanotubes Grafted CNTs as Electrocatalysts for Enhanced Oxygen Reduction Reaction. Advanced Materials Interfaces, 2022, 9, .	1.9	8
304	Formation energies of low-indexed surfaces of tin dioxide terminated by nonmetals. Solid State Communications, 2010, 150, 957-960.	0.9	7
305	Adsorption and Dissociation of Ammonia Borane Outside and Inside Single-Walled Carbon Nanotubes: A Density Functional Theory Study. Journal of Physical Chemistry C, 2011, 115, 12580-12585.	1.5	7
306	A remarkable two-dimensional membrane for multifunctional gas separation: halogenated metal-free fused-ring polyphthalocyanine. Physical Chemistry Chemical Physics, 2018, 20, 18931-18937.	1.3	7

#	ARTICLE	IF	CITATIONS
307	Strain induced variation of PFOS adsorption on pristine and defected phosphorene: A DFT study. Applied Surface Science, 2020, 532, 147452.	3.1	7
308	Regulating the interfacial behavior of carbon nanotubes for fast lithium storage. Electrochimica Acta, 2021, 388, 138591.	2.6	7
309	Molecular dynamic investigation of the structure and stress in crystalline and amorphous silicon during lithiation. Computational Materials Science, 2020, 183, 109811.	1.4	7
310	Nitrateâ€ŧoâ€Ammonia Conversion at an InSnâ€Enriched Liquidâ€Metal Electrode. Angewandte Chemie, 0, , .	1.6	7
311	GROWTH OF C36-FILMS ON DIAMOND SURFACE THROUGH MOLECULAR DYNAMICS SIMULATION. International Journal of Modern Physics B, 2002, 16, 3971-3978.	1.0	6
312	DFT study of electronic and optical properties of anatase titanium dioxide tuned by nitrogen and lithium co-doping. Solid State Communications, 2016, 228, 22-26.	0.9	6
313	Charging assisted structural phase transitions in monolayer InSe. Physical Chemistry Chemical Physics, 2017, 19, 22502-22508.	1.3	6
314	Two-Dimensional CuTe ₂ X (X = Cl, Br, and I): Potential Photocatalysts for Water Splitting under the Visible/Infrared Light. Journal of Physical Chemistry C, 2019, 123, 25543-25548.	1.5	6
315	Predicting ultrafast Dirac transport channel at the one-dimensional interface of the two-dimensional coplanar <mml:math xmlns:mml="http://www.w3.org/1998/Math/MathML"><mml:mrow><mml:mi>ZnO</mml:mi><mml:mo>/</mml:mo></mml:mrow></mml:math> <mml:mrow><mml:mi>ZnO</mml:mi><mml:mo>/znO<mml:mn>2</mml:mn></mml:mo></mml:mrow>	mar≯rum	:m&Mo
316	Predicting MnB6 monolayer with room temperature ferromagnetism and high magnetic anisotropy. Physica E: Low-Dimensional Systems and Nanostructures, 2021, 134, 114930.	1.3	6
317	N/P-Doped MoS ₂ Monolayers as Promising Materials for Controllable CO ₂ Capture and Separation under Reduced Electric Fields: A Theoretical Modeling. Journal of Physical Chemistry C, 2022, 126, 203-211.	1.5	6
318	Switchable topological phase transition and nonlinear optical properties in a <mml:math xmlns:mml="http://www.w3.org/1998/Math/MathML"><mml:mrow><mml:msub><mml:mi>ReC</mml:mi><mml mathvariant="normal">H</mml </mml:msub></mml:mrow> monolayer. Physical Review B, 2022, 105, .</mml:math 	:m n #2 <td>ımlamn></td>	ıml a mn>
319	Superb storage and energy saving separation of hydrocarbon gases in boron nitride nanosheets via a mechanochemical process. Materials Today, 2022, 57, 26-34.	8.3	6
320	Atypical Defect Motions in Brittle Layered Sodium Titanate Nanowires. Journal of Physical Chemistry Letters, 2018, 9, 6052-6059.	2.1	5
321	Polymorphism of low dimensional boron nanomaterials driven by electrostatic gating: a computational discovery. Nanoscale, 2020, 12, 10543-10549.	2.8	5
322	Two-Dimensional Janus Antimony Selenium Telluride with Large Rashba Spin Splitting and High Electron Mobility. ACS Omega, 2021, 6, 31919-31925.	1.6	5
323	hcp-phased Ni nanoparticles with generic catalytic hydrogenation activities toward different functional groups. Science China Materials, 2022, 65, 1252-1261.	3.5	5
324	Energy dependence of methyl-radical adsorption on diamond (001)-(2×1) surface. Surface and Coatings Technology, 2001, 141, 246-251.	2.2	4

#	Article	IF	CITATIONS
325	Structure character in small-carbon-cluster deposition on diamond surface. European Physical Journal D, 2003, 23, 369-373.	0.6	4
326	Structural and electronic properties of diazonium functionalized (4, 4) single walled carbon nanotube: an <i>ab initio</i> study. Molecular Simulation, 2006, 32, 1213-1217.	0.9	4
327	Reversible Intercalation of Multivalent Al 3+ Ions into Potassiumâ€Rich Cryptomelane Nanowires for Aqueous Rechargeable Alâ€Ion Batteries. ChemSusChem, 2019, 12, 3670-3670.	3.6	4
328	Functionalized boron nitride monolayers as promising materials for uranyl ion capture: A first-principles study. Journal of Molecular Structure, 2020, 1200, 127080.	1.8	4
329	<scp>N₂</scp> electrochemical reduction on two dimensional transition metal monoborides: A density functional theory study. International Journal of Quantum Chemistry, 2021, 121, e26548.	1.0	4
330	CO ₂ Capture, Separation and Reduction on Boronâ€Doped MoS ₂ , MoSe ₂ and Heterostructures with Different Doping Densities: A Theoretical Study. ChemPhysChem, 2021, 22, 2392-2400.	1.0	4
331	Interfacing 2D VS2 with Janus MoSSe: Antiferromagnetic electric polarization and charge transfer driven Half-metallicity. Applied Surface Science, 2021, 570, 151129.	3.1	4
332	Versatile Gold Telluride Iodide Monolayer as a Potential Photocatalyst for Water Splitting. Nanomaterials, 2022, 12, 1915.	1.9	4
333	Impact energy dependence of Al13 cluster deposition on Ni(001) surface. Surface Science, 2002, 512, 128-134.	0.8	3
334	Adatom CCV Auger rates via the local density of states. Surface Science, 2003, 545, L753-L760.	0.8	3
335	Half metallicity in a zigzag double-walled nanotube nanodot: An ab initio prediction. Chemical Physics Letters, 2009, 468, 257-259.	1.2	3
336	Mechanism of ferromagnetism in non-magnetic ion-doped zinc oxides. Physica Scripta, 2014, 89, 015807.	1.2	3
337	Anomalous Enhancement of Mechanical Properties in the Ammonia Adsorbed Defective Graphene. Scientific Reports, 2016, 6, 33810.	1.6	3
338	Water Splitting: In Situ Formation of Oxygen Vacancies Achieving Nearâ€Complete Charge Separation in Planar BiVO ₄ Photoanodes (Adv. Mater. 26/2020). Advanced Materials, 2020, 32, 2070198.	11.1	3
339	First principles studies of mononuclear and dinuclear Pacman complexes for electrocatalytic reduction of CO2. Catalysis Science and Technology, 2021, 11, 637-645.	2.1	3
340	Controllable Acceleration and Deceleration of Charge Carrier Transport in Metalâ€Halide Perovskite Singleâ€Crystal by Csâ€Cation Induced Bandgap Engineering. Small, 2022, 18, e2107680.	5.2	3
341	The location of Ti atom in sodium alanate: an ab initio spin-polarised study. International Journal of Nanotechnology, 2007, 4, 564.	0.1	2
342	Hydrogen trapping in MAX phase Ti ₃ SiC ₂ : Insight from chemical bonding by density functional theory. Europhysics Letters, 2017, 118, 47002.	0.7	2

#	Article	IF	CITATIONS
343	Predicting the strain-mediated topological phase transition in 3D cubic ThTaN ₃ . Beilstein Journal of Nanotechnology, 2018, 9, 1399-1404.	1.5	2
344	A Highly Efficient Conjoinedâ€ŧwin Porphyrinâ€based Complex for the Electrochemical Reduction of CO to Ethanol. ChemNanoMat, 2021, 7, 935-941.	1.5	2
345	2D Nanomaterials: Moleculeâ€Induced Conformational Change in Boron Nitride Nanosheets with Enhanced Surface Adsorption (Adv. Funct. Mater. 45/2016). Advanced Functional Materials, 2016, 26, 8356-8356.	7.8	1
346	Exploring Aluminumâ€lon Insertion into Magnesiumâ€Doped Manjiroite (MnO 2) Nanorods in Aqueous Solution. ChemElectroChem, 2021, 8, 995-995.	1.7	0
347	Numerical investigation of microstructure and failure of lithiated silicon under biaxial tension. Computational Materials Science, 2021, 200, 110764.	1.4	0